AUCTORES
Globalize your Research

International Journal of Clinical Case Reports and Reviews
Nan Lu *

Open Access

Review Article

Theoretical investigation on Cu/Pd-catalyzed domino radical cyclization and C–H carbonylation of α-bromocarbonyl leading to carbonyl-containing quinolin-2(1H)-one scaffold

Nan Lu *, and Chengxia Miao

College of Chemistry and Material Science, Shandong Agricultural University, Taian 271018, P. R. China.

***Corresponding Author:** Nan Lu, College of Chemistry and Material Science, Shandong Agricultural University, Taian 271018, P. R. China.

Received Date: December 18, 2024 | **Accepted Date:** January 23, 2025 | **Published Date:** February 04, 2025

Citation: Nan Lu, and Chengxia Miao, (2025), Theoretical investigation on Cu/Pd-catalyzed domino radical cyclization and C−H carbonylation of α-bromocarbonyl leading to carbonyl-containing quinolin-2(1H)-one scaffold, *International Journal of Clinical Case Reports and Reviews*, 23(1); **DOI:**10.31579/2690-4861/652

Abstract:

Our DFT calculations provide the first theoretical investigation on Cu/Pd-catalyzed domino radical cyclization and C−H carbonylation of α-bromocarbonyl. The SET reduction was induced by CuI attacking C−Br of α-bromocarbonyl generating CuIIBr followed by intramolecular radical addition generating six-membered ring. The alkenyl bromide was formed assisted by CuIIBr together with CuI regeneration. Next, alkenyl PdII was giv-en via oxidative addition of Pd0 to C-Br. The five-membered cyclic PdII was obtained via intramolecular C−H activation. Finally, two paths are competitive to furnish six-membered acyl PdII via insertion of CO to C-Pd bond. The polycyclic carbonyl-containing quinolin-2(1H)-one was yielded via reductive elimination squeezing recovered Pd0 from six-membered ring. CO insertion is determined to be rate-limiting. The positive solvation effect is suggested by decreased absolute and activation energies in solution compared with in gas. These results are supported by Multiwfn analysis on FMO composition of specific TSs, and MBO value of vital bonding, breaking.

Key words: radical cyclization; C−H carbonylation; α-bromocarbonyl; quinolin-2(1H)-one; CO insertion

1.Introduction

As a fascinating way in organic synthesis, domino reactions are the most powerful method to prepare complex polycyclic system with excellent chemo-, regio-, and enantioselectivity [1]. This efficient process consists of several catalytic bond-forming transformations starting from simple substrates [2]. Especially, the pericyclic domino reactions have provided concise and straightforward approaches to natural carbocyclic frameworks [3]. Many progresses were achieved in past few decades. Che reported a facile access to ketones from aldehydes through copper-catalyzed cascade annulation of unsaturated α-bromocarbonyls with enynals [4]. Fu discovered Rh-catalyzed [4 + 2] annulation with monodentate structure toward iminopyranes and pyranones by C-H annulation [5]. Chen found three-component fusion to pyrazolo[5,1-a]isoquinolines and N-naphthyl pyrazoles via Rh-catalyzed multiple order transformation ofenaminones or Satoh-Miura benzannulation [6,7]. Kanganavaree researched Palladium-catalyzed double decarboxylative [3 + 2] annulation of naphthalic anhydrides with internal alkynes [8].

On the other hand, polycyclic quinolin-2(1H)-ones are ubiquitous scaffolds in natural products and pharmaceutical agents exhibiting diverse biological activities such as novel insecticidal antibiotics from Penicillium sp. FKI-2140 of yaequinolones J1 and J2 [9], the related dioxoaporphines of cepharadiones A,B [10] and the melodinus alkaloid (+)-meloscine [11]. What's more, the derivatives can serve as key intermediates to produce complex polycyclic heterocycles [12]. In this field, domino reactions using alkyne-tethered α-bromocarbonyls are the most fascinated approach. For example, Kang developed synthesis of quinolin-2-ones and quinoline-2,4-diones through copper-catalyzed cyclization [13]. Li group discovered copper-catalyzed domino annulation with alkynes to construct 1H-benzo[de]quinolin-2(3H)-ones, 4H-dibenzo[de,g]quinolin-5(6H)-ones and benzo[de]chromen-2(3H)-ones as well as the cyclopenta[de]-quinoline-2,5(1H,3H)-diones via a rhodium-catalyzed tandem cyclization and C−H carbonylation [14,15]. Xue group realized simultaneous construction of heterocyclic scaffold and introduction of acyl group in synthesis of acyl

cyclopentaquinolinones and visible light-induced radicalcyclization leading to O-heterocycle spiro-fused cyclopentaquinolinones, cyclopentaindenes [16,17]. There are also ultrafast construction of 2-quinolinone-fused γ-lactones and visible-light-promoted tandem annulation of N-(o-ethynylaryl) acrylamides with CH_2Cl_2 [18,19].

In recent years, Ying group obtained a series of achievements owing to their continued interest in domino carbonylative reaction. The main outcomes are Nickel-catalyzed cascade carbonylative synthesis of N-benzoyl indoles, Nickel-catalyzed carbonylative domino cyclization of arylboronic acid pinacol esters, Palladium-catalyzed case of perfluoroalkyl, carbonyl-containing 3,4-dihydroquinolin-2(1H)-one and polycyclic 3,4-dihydroquinolin-2(1H)-one scaffolds [20-24]. A novel breakthrough we are interested in was Cu/Pd-catalyzed domino radical cyclization and C−H carbonylation of α-bromocarbonyls [25]. Although a variety of polycyclic carbonyl-containing quinolin-2(1H)-one derivative were obtained, many problems still puzzled and there was no report about detailed mechanistic study explaining the rapid incorporation of CO into polycyclic quinolin-2(1H)-one. How active Cu^{I} and $Cu^{II}Br$ function in SET reduction and intramolecular radical addition? What's the role of active Pd^{0} in oxidative addition and intramolecular C−H activation giving alkenyl Pd^{II} intermediate and cyclic Pd^{II} complex? Why two competitive paths exist in final CO insertion and reductive elimination via acyl Pd^{II} intermediate to target product? To solve these problems in experiment, an in-depth theoretical study was necessary for this strategy.

2 Computational details

The geometry optimizations were performed at the B3LYP/BSI level with the Gaussian 09 package [26,27]. The mixed basis set of LanL2DZ for Cu, Pd, Br and 6-31G(d) for other non-metal atoms [28-32] was denoted as BSI. Different singlet and multiplet states were clarified with B3LYP and ROB3LYP approaches including Becke's three-parameter hybrid functional combined with Lee−Yang−Parr correction for correlation [33,34]. The nature of each structure was verified by performing harmonic vibrational frequency calculations. Intrinsic reaction coordinate (IRC) calculations were examined to confirm the right connections among key transition-states and corresponding reactants and products. Harmonic frequency calculations were carried out at the B3LYP/BSI level to gain zero-point vibrational energy (ZPVE) and thermodynamic corrections at 383 K and 1 atm for each structure in dimethylsulfoxide (DMSO). The solvation-corrected free energies were obtained at the B3LYP/6-311++G(d,p) (LanL2DZ for Cu, Pd, Br) level by using integral equation formalism polarizable continuum model (IEFPCM) in Truhlar's "density" solvation model [35-37] on the B3LYP/BSI-optimized geometries.

As an efficient method of obtaining bond and lone pair of a molecule from modern ab initio wave functions, NBO procedure was performed with Natural bond orbital (NBO3.1) to characterize electronic properties and bonding orbital interactions [38,39]. The wave function analysis was provided using Multiwfn_3.7_dev package [40] including research on frontier molecular orbital (FMO) and Mayer bond order (MBO).

3 Results and Discussion

The mechanism was explored for (Scheme 1). Illustrated by black arrow of Scheme 2, the SET reduction was initially induced by active Cu^{I} species attacking the C−Br bond of α-bromocarbonyl **1** generating radical **A** and $Cu^{II}Br$ species. Then from **A**, the intramolecular radical addition gave another radical **B** (red arrow). Next, the alkenyl bromide **3** was formed via reaction of **B** with $Cu^{II}Br$ species together with the regeneration of active Cu^{I} species. Subsequently, via oxidative addition of active Pd^{0} species to **3**, the alkenyl Pd^{II} intermediate **C** was produced, the intramolecular C−H activation of which took place affording the cyclic Pd^{II} complex **D** under the influence of base (blue arrow). Two competitive paths A (magenta arrow) and B (green arrow) are expected to furnish acyl Pd^{II} intermediate **E** or **F** via insertion of CO to **D**. Finally, the target product polycyclic quinolin-2(1H)-one **2** was yielded via reductive elimination of **E** or **F** and Pd^{0} species was recovered for next catalytic cycle.

The schematic structures of optimized TSs in Scheme 2 were listed by Figure 1. The activation energy was shown in Table 1 for all steps. Supplementary Table S1, Table S2 provided the relative energies of all stationary points. According to experiment, the Gibbs free energies in DMSO solution phase are discussed here.

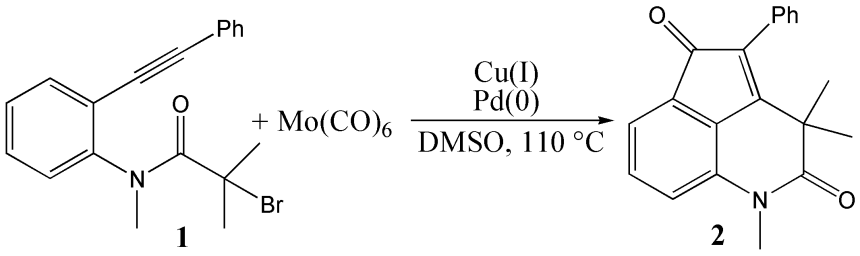

Scheme 1 Cu/Pd-catalyzed domino radical cyclization and C−H carbonylation of α-bromocarbonyl **1** leading to carbonyl-containing quinolin-2(1H)-one **2**.

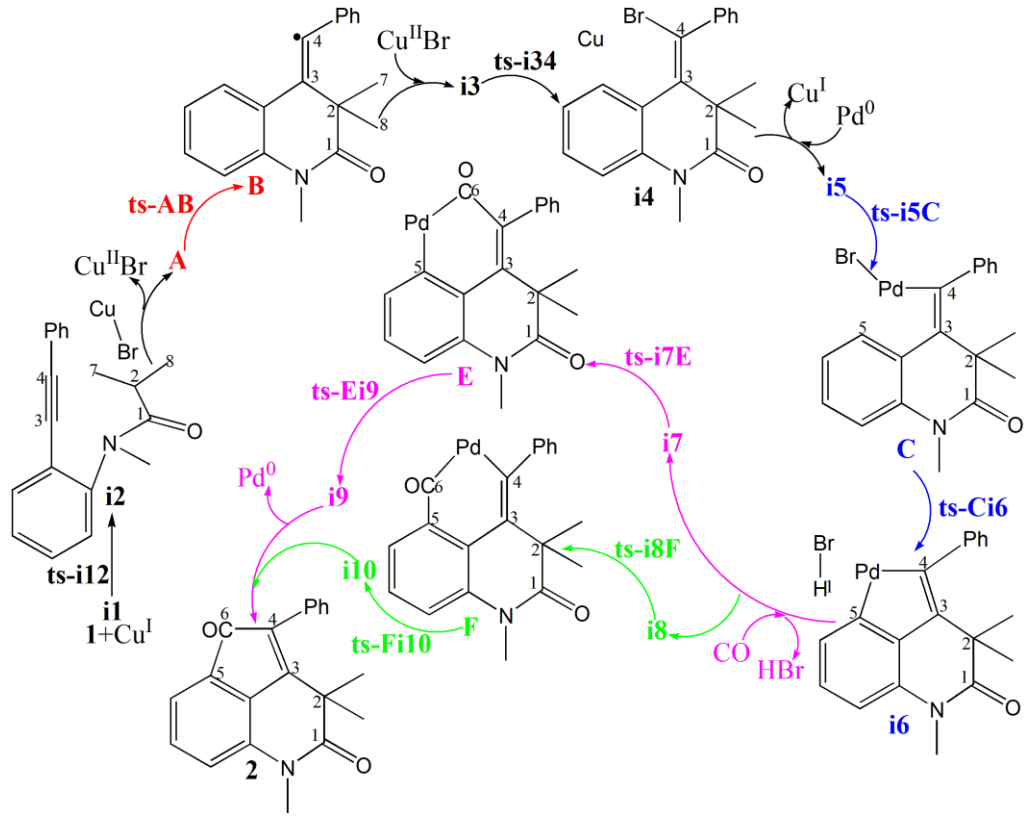

Scheme 2: Proposed reaction mechanism of Cu/Pd-catalyzed domino radical cyclization and C−H carbonylation of **1** affording **2**. TS is named according to the two intermediates it connects.

TS	$\Delta G^{\neq}_{gas}$	$\Delta G^{\neq}_{sol}$
ts-i12	19.9	8.8
ts-AB	2.6	6.0
ts-i34	22.9	9.5
ts-i5C	2.2	1.6
ts-Ci6	26.0	25.7
ts-i7E	41.4	37.6
ts-Ei9	13.4	14.2
ts-i8F	48.3	42.9
ts-Fi10	18.1	17.5

(a)

Table 1: The activation energy (in kcal mol^{-1}) of all reactions in gas and solvent

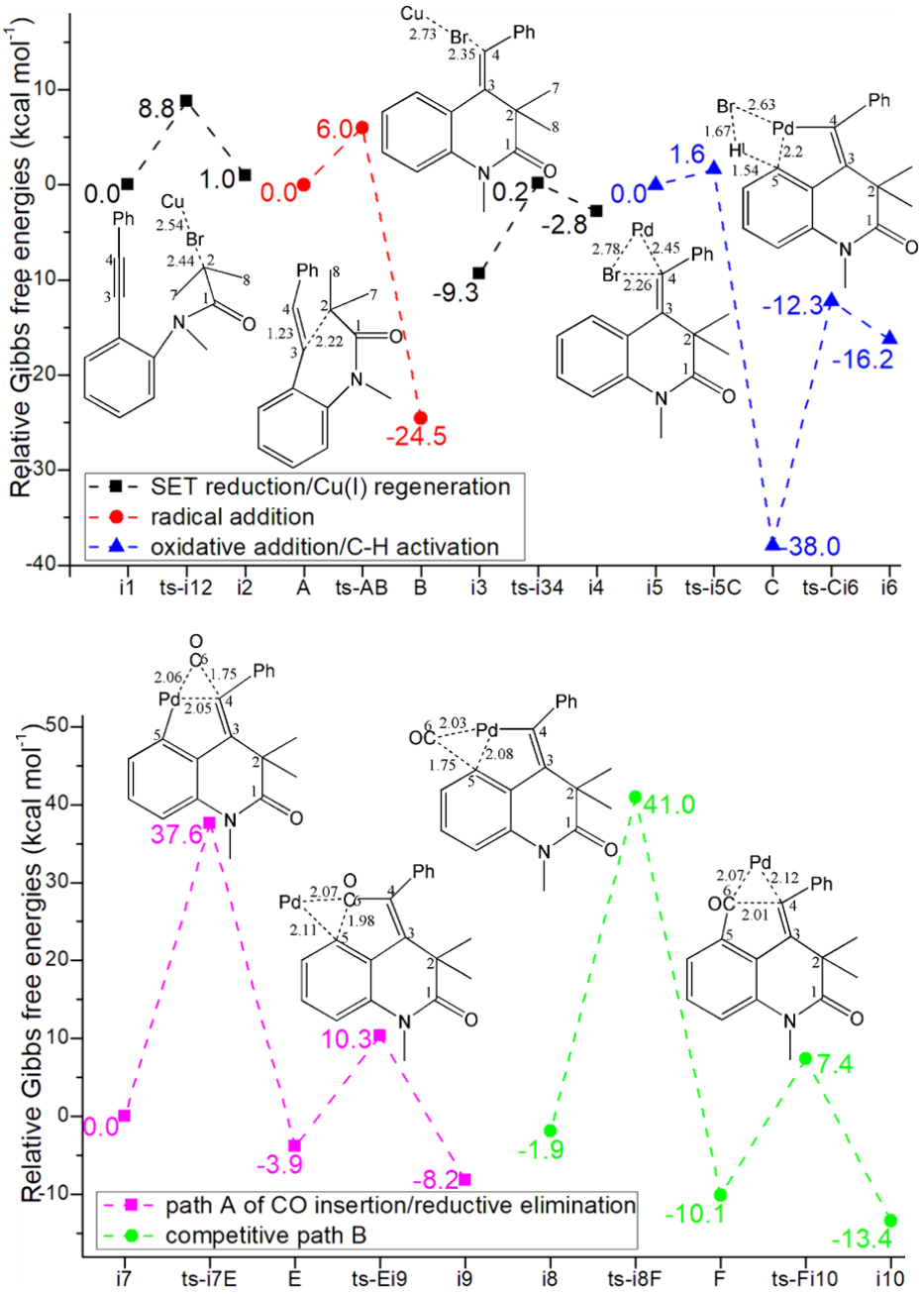

Figure 1: Relative Gibbs free energy profile in solvent phase starting from complex (a) **i1**, **A**, **i5** (b) **i7** (Bond lengths of optimized TSs in Å).

3.1 SET reduction/intramolecular radical addition/Cu^{I} regeneration

Initially with active Cu^{I} species, α-bromocarbonyl **1** forms **i1** as starting point (black dash line of Fig. 1a). The SET reduction was induced by Cu^{I} attacking C2−Br bond via **ts-i12** in step 1 with the activation energy of 8.8 kcal mol^{-1} slightly endothermic by 1.0 kcal mol^{-1} generating **i2**. The transition vector denotes simultaneous cleavage of C2···Br and Cu···Br linkage (2.44, 2.54 Å). In **i2**, one electron is located on C2 in resultant radical **A** together with $Cu^{II}Br$ species.

Then from **A**, the intramolecular radical addition proceeds via **ts-AB** in step 2 with activation energy of 6.0 kcal mol^{-1} affording another radical **B** exothermic by -24.5 kcal mol^{-1} (red dash line of Fig. 1a). According to the transition vector, the reactive C2 is attacking positive alkyne C3 making triple bond C3≡C4 stretching to double one (2.22, 1.23 Å) (Figure S1a). **B** is more stable than **A** with the newly closed six membered ring and the single electron transferring to C4.

Next with $Cu^{II}Br$ species, **B** forms **i3** involving relative energy increased by 15.2 kcal mol^{-1} easily to initiate step 3. Thus C4 is attacked as expected via **ts-i34** with activation energy of 9.5 kcal mol^{-1} exothermic a little by -2.8 kcal mol^{-1} giving intermediate **i4**. The transition vector describes a reverse process with that of **ts-i12**, that is Cu···Br breaking and C4···Br bonding (2.73, 2.35 Å) (Figure S1b). Once typical C4-Br single bond is formed, the key alkenyl bromide compound **3** was obtained along with the regeneration of active Cu^{I} species.

3.2 Oxidative addition/intramolecular C−H activation

Subsequently, **i5** is located as new starting point of next two steps with the removal of Cu^{I} and additional Pd^{0} species to **3** (blue dash line of Fig.

1a). The oxidative addition takes place via **ts-i5C** in step 4 with small activation energy of 1.6 kcal mol^{-1} exothermic huge by -38.0 kcal mol^{-1} giving stable alkenyl Pd^{II} intermediate **C**. The transition vector corresponds to insertion of active Pd^0 to C4-Br single bond that is concerted dissociation of C4···Br, bonding of C4···Pd and Pd···Br (2.26, 2.45, 2.78 Å) (Figure S1c). The oxidation of Pd^0 to Pd^{II} is quite favorable both kinetically and thermodynamically.

Under the influence of base, intramolecular C5−H1 activation on benzene ring is achieved via **ts-Ci6** in step 5 with activation energy of 25.7 kcal mol^{-1} exothermic by -16.2 kcal mol^{-1} affording **i6**. The activated H1 is likely to connect with adjacent Br forming HBr molecule just as the description by transition vector, which includes breaking of Pd···Br, C5···H1 and the later linkage of Pd···C5, H1···Br. When the typical Pd-C5 single bond is formed in **i6**, a new five membered cyclic Pd^{II} complex **D** is available after the removal of isolated HBr.

3.3 CO insertion/reductive elimination

The following two steps involves participation of CO provided by $Mo(CO)_6$. Two paths A and B are feasible to furnish acyl Pd^{II} intermediate **E** or **F**. Path A is initiated from **i7** binding CO and **D** as new starting point of next two steps (magenta dash line of Fig. 1b). The insertion of CO to **D** occurs via **ts-i7E** in step 6 with increased activation energy of 37.6 kcal mol^{-1} exothermic by -3.9 kcal mol^{-1} delivering **E** characterized by expanded six membered ring. The detailed atomic motion is illustrated according to the transition vector about insertion of O≡C6 to C4-Pd single bond comparising simultaneous broken of C4···Pd and connection of C4···C6, C6···Pd (2.05, 1.75, 2.06 Å) (Figure S1d).

In step 7, the reductive elimination from **E** proceeds via **ts-Ei9** with mediate activation energy of 14.2 kcal mol^{-1} exothermic by -8.2 kcal mol^{-1} generating complex **i9** binding target product polycyclic quinolin-2(1H)-one **2** and recovered Pd^0 species for next catalytic cycle. The transition vector corresponds to the extrusion of Pd^0 from six membered ring, which consists of previous stretching of C5···Pd, C6···Pd and the resulting linkage of C5···C6 in detail (2.11, 2.07, 1.98 Å) (Figure S1e). The final five membered ring of **2** is closed depending on the formation of C5-C6 single bond.

For alternative path B (green dash line of Fig. 1b), the CO insertion is via **ts-i8F** with activation energy of 42.9 kcal mol^{-1} exothermic by -10.1 kcal mol^{-1} delivering **F**. The transition vector reveals insertion of O≡C6 to C5-Pd involving C5···Pd broken and C5···C6, C6···Pd connection (2.08, 1.75, 2.03 Å). The next reductive elimination is via **ts-Fi10** with activation energy of 17.5 kcal mol^{-1} exothermic by -13.4 kcal mol^{-1} intermediate yielding **i10**. The transition vector suggests Pd^0 is squeezed between C4, C6 via elongation of C4···Pd, C6···Pd and C4···C6 connection (2.12, 2.07, 2.01 Å).

Although the relative energies of stationary points on path B are mostly lower than those of counterparts on path A, the barriers are both higher for two steps of path B confirming the slightly disadvantage from kinetics. Comparatively, CO insertion of step 6 is determined to be rate-limiting for the whole process. To highlight the idea of feasibility for changes in electron density and not molecular orbital interactions are responsible of the reactivity of organic molecules, quantum chemical tool Multiwfn was applied to analyze of electron density such as MBO results of bonding atoms and contribution of atomic orbital to HOMO of typical TSs (Table S3, Figure S2). These results all confirm the above analysis.

4 Conclusions

Our DFT calculations provide the first theoretical investigation on Cu/Pd-catalyzed domino radical cyclization and C−H carbonylation of α-bromocarbonyl. The SET reduction was initially induced by active Cu^I species attacking C−Br bond of α-bromocarbonyl generating $Cu^{II}Br$ species and radical followed by intramolecular radical addition generating closed six membered ring. The alkenyl bromide was formed assisted by $Cu^{II}Br$ species together with regeneration of active Cu^I. Next, the alkenyl Pd^{II} intermediate was given via oxidative addition of active Pd^0 species to C-Br bond. The five membered cyclic Pd^{II} complex was obtained via intramolecular C−H activation under the influence of base. Finally, two feasible paths are competitive to furnish two six membered acyl Pd^{II} intermediates via insertion of CO to different C-Pd bond. The target product polycyclic carbonyl-containing quinolin-2(1H)-one was yielded via reductive elimination squeezing recovered Pd^0 from six membered ring. CO insertion is determined to be rate-limiting for the whole process. The positive solvation effect is suggested by decreased absolute and activation energies in DMSO solution compared with in gas. These results are supported by Multiwfn analysis on FMO composition of specific TSs, and MBO value of vital bonding, breaking.

Electronic Supplementary Material

Supplementary data available: [Computation information and cartesian coordinates of stationary points; Calculated relative energies for the ZPE-corrected Gibbs free energies (ΔG_{gas}), and Gibbs free energies (ΔG_{sol}) for all species in solution phase at 383 K.]

Author contributions: Conceptualization, Nan Lu; Methodology, Nan Lu; Software, Nan Lu; Validation, Nan Lu; Formal Analysis, Nan Lu; Investigation, Nan Lu; Resources, Nan Lu; Data Curation, Nan Lu; Writing-Original Draft Preparation, Nan Lu; Writing-Review & Editing, Nan Lu; Visualization, Nan Lu; Supervision, Chengxia Miao; Project Administration, Chengxia Miao; Funding Acquisition, Chengxia Miao. All authors have read and agreed to the published version of the manuscript.

Funding: This work was supported by National Natural Science Foundation of China (21972079) and Key Laboratory of Agricultural Film Application of Ministry of Agriculture and Rural Affairs, P.R. China.

Conflict of interest: The authors declare no conflict of interest.

References

1. Tietze, L. F. (1996). Domino reactions in organic synthesis. Chem. Rev. 96, 115−136.
2. Tietze, L. F.; Modi, A. (2000). Multicomponent domino reactions for the synthesis of biologically active natural products and drugs. Med. Res. Rev. 20, 304−322.
3. Poulin, J.; Grise-Bard, C. M.; Barriault, L. (2009). Pericyclic domino reactions: concise approaches to natural carbocyclic frameworks. Chem. Soc. Rev. 38, 3092−3101.
4. Che, C.; Huang, Q.; Zheng, H.; Zhu, G. (2016). Copper-catalyzed cascade annulation of unsaturated α-bromocarbonyls with enynals: a facile access to ketones from aldehydes. Chem. Sci.7, 4134−4139.
5. Fu, L.; Xu, W.; Pu, M.; Wu, Y.-D.; Liu, Y. et al. (2022). Rh-catalyzed [4 + 2] annulation with a removable monodentate structure toward iminopyranes and pyranones by C-H annulation. Org. Lett.24, 3003−3008.

6. Chen, D.; Wan, C.; Liu, Y.; Wan, J.-P. (2023). Three-component fusion to pyrazolo[5,1-a]isoquinolines via Rh-catalyzed multiple order transformation ofenaminones. *J. Org. Chem*. 88, 4833−4838.
7. Chen, D.; Zhou, L.; Liu, Y.; Wan, J.-P. (2023). Three-component synthesis of N-naphthyl pyrazoles via Rh(III)-catalyzed cascade pyrazole annulation and Satoh-Miura benzannulation. Chem. Commun. 59, 4036−4039.
8. Kanganavaree, C.; Kantarod, K.; Worakul, T.; Soorukram, D.; Kuhakarn, C. et al. (2024). Palladium-catalyzed double decarboxylative [3 + 2] annulation of naphthalic anhydrides with internal alkynes. *J. Org. Chem.* 89, 15083−15090.
9. Uchida, R.; Imasato, R.; Shiomi, K.; Tomoda, H.; Ōmura, S. (2005). Yaequinolones J1 and J2, novel insecticidal antibiotics from Penicillium sp. FKI-2140. Org. Lett. 7, 5701−5704.
10. Elban, M. A.; Chapuis, J. C.; Li, M.; Hecht, S. M. (2007). Synthesis and biological evaluation of cepharadiones A and B and related dioxoaporphines. Bioorg. Med. Chem. 15, 6119−6125.
11. Selig, P.; Bach, T. (2008). Enantioselective total synthesis of the melodinus alkaloid (+)-meloscine. Angew. Chem., Int. Ed. 47, 5082−5084.
12. Li, Q.; Cai, Y.; Hu, Y.; Jin, H.; Chen, F. et al. (2021). Nickel-catalyzed cyclization of 1,7-enynes for the selective synthesis of dihydrocyclobuta[c]quinolin-3-ones and benzo[b]azocin-2-ones. Chem. Commun. 57, 11657−11660.
13. Kang, Q.; Wang, Z.; Hu, S.; Luo, C.; Cai, X. et al. (2022). Copper-catalyzed switchable cyclization of alkyne-tethered α-bromocarbonyls: selective access to quinolin-2-ones and quinoline-2,4-diones. Org. Chem. Front. 9, 6617−6623.
14. Liu, B.; Yu, J.; Li, Y.; Li, J.; He, D. (2018). Copper-catalyzed annulation cascades of alkyne-tethered α-bromocarbonyls with alkynes: an access to heteropolycycles. Org. Lett. 20, 2129−2132.
15. Yang, Y.; He, D.; Li, J. (2021). Rhodium-catalyzed reductive trans-alkylacylation of internal alkynes via a formal carborhodation/C-H carbonylation cascade. Org. Lett. 23, 5039−5043.
16. Xue, L.; Gao, C.; Zhang, X.; Fan, X. (2024). Synthesis of acyl cyclopentaquinolinones through simultaneous construction of the heterocyclic scaffold and introduction of the acyl group. J. Org. Chem. 89, 6292−6305.
17. Xue, L.; Song, X.; Zhang, X.; Fan, X. (2023). Synthesis of O-heterocycle spiro-fused cyclopentaquinolinones and cyclopentaindenes through visible light-induced radicalcyclization reactions. *J. Org. Chem*. 88, 12641−12657.
18. Sacchelli, B. A. L.; Rocha, B. C.; Andrade, L. H. (2021). Cascade reactions assisted by microwave irradiation: ultrafast construction of 2-quinolinone-fused γ-lactones from N-(o-ethynylaryl)acrylamides and formamide. Org. Lett. 23, 5071−5075.
19. Liu, Y.; Song, R.-J.; Luo, S.; Li, J.-H. (2018). Visible-light-promoted tandem annulation of N-(o-ethynylaryl)acrylamides with CH2Cl2. Org. Lett. 20, 212−215.
20. Yao, L.; Ying, J.; Wu, X. (2021). Nickel-catalyzed cascade carbonylative synthesis of N-benzoyl indoles from 2-nitroalkynes and aryl iodides. Org. Chem. Front. 8, 6541−6545.
21. Wang, S.; Zhang, J.; Wang, J.; Ying, J.; Wu, X. (2022). Palladium-catalyzed cascade carbonylative synthesis of perfluoroalkyl and carbonyl-containing 3,4-dihydroquinolin-2(1H)-one derivatives. Org. Lett. 24, 8843−8847.
22. Yao, L.; Wei, P.; Ying, J.; Wu, X. (2022). Nickel-catalyzed carbonylative domino cyclization of arylboronic acid pinacol esters with 2-alkynyl nitroarenes toward N-aroyl indoles. Org. *Chem. Front.* 9, 2685−2689.
23. Wang, J.; Zhang, J.; Wang, S.; Ying, J.; Li, C. et al. (2022). Palladium-catalyzed domino carbonylative cyclization to access functionalized heterocycles. *J. Catal*. 414, 313−318.
24. Wang, S.; Zhao, J.; Ying, J.; Wu, X. (2023). Palladium-catalyzed carbonylative synthesis of polycyclic 3,4-dihydroquinolin-2(1H)-one scaffolds containing perfluoroalkyl and carbonyl units. Org. Lett. 25, 5314−5318.
25. Wang, J.; Wang, S.; Li, S.; Zhao, J.; Ying, J. Cu/Pd-Catalyzed Domino Carbonylative Synthesis of Polycyclic Carbonyl-Containing Quinolin-2(1H)-one Scaffolds from α-Bromocarbonyls. J. Org. Chem. doi.org/10.1021/acs.joc.4c02551
26. Frisch, M. J.; Trucks, G. W.; Schlegel, H. B. et al. (2010). Gaussian 09 (Revision B.01), Gaussian, Inc., Wallingford, CT.
27. Hay, P. J.; Wadt, W. R. (1985). Ab initio effective core potentials for molecular calculations-potentials for the transition-metal atoms Sc to Hg. J. Chem. Phys. 82, 270-283.
28. Lv, H.; Han, F.; Wang, N.; Lu, N.; Song, Z. et al. (2022). Ionic Liquid Catalyzed C-C Bond Formation for the Synthesis of Polysubstituted Olefins. *Eur. J. Org*. Chem. e202201222.
29. Zhuang, H.; Lu, N.; Ji, N.; Han, F.; Miao, C. (2021). Bu4NHSO4-Catalyzed Direct N-Allylation of Pyrazole and its Derivatives with Allylic Alcohols in Water: A Metal-free, Recyclable and Sustainable System. Advanced Synthesis & Catalysis. 363, 5461-5472.
30. Lu, N.; Lan, X.; Miao, C.; Qian, P. (2020). Theoretical investigation on transformation of Cr(II) to Cr(V) complexes bearing tetra-NHC and group transfer reactivity. *Int. J. Quantum Chem*. 120, e26340.
31. Lu, N.; Liang, H.; Qian, P.; Lan, X.; Miao, C. (2020). Theoretical investigation on the mechanism and enantioselectivity of organocatalytic asymmetric Povarov reactions of anilines and aldehydes. *Int. J. Quantum Chem*. 120, e26574.
32. Lu, N.; Wang, Y. (2023). Alloy and Media Effects on the Ethanol Partial Oxidation Catalyzed by Bimetallic Pt6M (M= Co, Ni, Cu, Zn, Ru, Rh, Pd, Sn, Re, Ir, and Pt). Computational and Theoretical Chemistry, 1228, 114252.
33. Catellani, M.; Mealli, C.; Motti, E.; Paoli, P.; Perez-Carren˜o, E. et al. (2002). Palladium-Arene Interactions in Catalytic Intermediates: An Experimental and Theoretical Investigation of the Soft Rearrangement between η1 and η2 Coordination Modes. *J. AM. CHEM*. SOC. 124, 4336-4346.
34. Marenich, A. V.; Cramer, C. J.; Truhlar, D. G. (2009). Universal Solvation Model Based on Solute Electron Density and on a Continuum Model of the Solvent Defined by the Bulk Dielectric Constant and Atomic Surface Tensions. *J. Phys. Chem*. B, 113, 6378–6396.
35. Tapia, O. (1992). Solvent effect theories: Quantum and classical formalisms and their applications in chemistry and biochemistry. *J. Math. Chem*. 10, 139-181.
36. Tomasi, J.; Persico, M.(1994). Molecular Interactions in Solution: An Overview of Methods Based on Continuous Distributions of the Solvent. Chem. Rev. 94, 2027-2094.
37. Tomasi, J.; Mennucci, B.; Cammi, R. (2005). Quantum Mechanical Continuum Solvation Models. Chem. Rev.105, 2999-3093.
38. Reed, A. E.; Weinstock, R. B.; Weinhold, F. (1985). Natural population analysis. J. Chem. Phys.83, 735-746.
39. Reed, A. E.; Curtiss, L. A.; Weinhold, F. (1988). Intermolecular interactions from a natural bond orbital donor-acceptor view point. Chem. Rev. 88, 899-926.
40. Lu, T.; Chen, F. (2012). Multiwfn: A multifunctional wavefunction analyzer. J. Comput. Chem.33, 580-592.

DOI:10.31579/2690-4861/652